Development of 3D two-photon acousto-optical measurement methods for neuroscience studies

PhD thesis

Szalay Gergely

Semmelweis University
Szentágothai János Doctoral School

Supervisor: Dr. Rózsa Balázs, M.D., Ph.D.

Official reviewers: Dr. Szabadics János, Ph.D.
Dr. Kis Petik Katalin, Ph.D.

Head of the Final Ex. Committee: Dr. Kellermayer Miklós, M.D., DSc
Members of the Final Ex. Committee: Dr. Tretter László, M.D., DSc
Dr. Ulbert István, M.D., DSc

Budapest
2018

Abstract

To better understand neuronal computation fast readout of information flow and processing is essential since action potentials, dendritic integration, subthreshold EPSP and IPSP events all happen at the millisecond timescale. Moreover, neuronal diversity, layer specificity of information processing, area-wise specialization of neuronal mechanisms, internally generated patterns, and dynamic network properties all suggest that fast recording is required not only from a single plane or point, but also at a level of large neuronal populations situated in large 3D volume. In addition, coding and computation within neuronal networks are generated not only by the somatic integration domains, but also by highly non-linear dendritic integration centers, which in most cases remain hidden from somatic recordings. Therefore, to get better insight in the details of these functions we need to simultaneously read out neural activity both at the population and single-cell levels, with sufficient spatial (in the μm range) and temporal (at the millisecond scale) resolution.

Introduction

Acousto-optical two-photon fluorescent imaging

Two-photon fluorescent imaging allows light base detection of neuronal activity deep in the tissue with great optical resolution. In the field of fluorescent imaging we use acousto-optical devices to diffract laser beams through ultrasonic gratings. The acousto-optical effect is based on a periodic change of the refractive index in a high refractive index medium, which is the result of the sound wave induced pressure fluctuation in the crystal. This grating diffracts the light beam just like a normal optical grating, but here the gradient can be rapidly adjusted by changing the driving signal.

Acousto-optic (AO) scanning technology could be used to rapidly change beam focusing without mechanical movement enabling the nearly simultaneous measurement of hundreds of scanning point distributed in a 3D volume.

Acousto-optical deflection

Acousto-optical deflectors (AODs) control the optical beam spatially, they use ultrasonic waves to diffract the laser beam depending on the acoustic frequency. If we introduce a sine wave at the piezoelectric driver, it will generate an optical deflection in the acousto-optic medium according to the following equation: $\Delta\Theta_d = \lambda/v * \Delta f$, where λ is the wavelength of the optical beam, v is the velocity of the acoustic wave, and Δf is the change in the sound frequency.

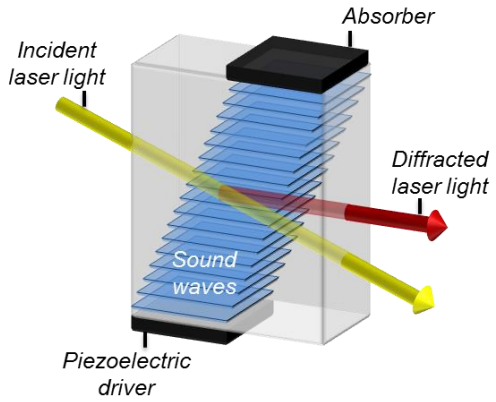

Operating principle of acousto-optical deflectors. *A piezoelectric driver elicits radio frequency sound waves due to the externally applied sinusoidal voltage. Sound enters and traverses through the diffracting medium while interacting with light throughout the aperture. Light is diffracted on the sound wave's refraction index changes as on a steady optical grating providing diffracted light beams whose angle is dependent on the sound wave's frequency.*

3D scanning configurations

Combining four of these crystals can form a 3D focusing system. We need two orthogonal deflectors for X and Y scanning, a third one for Z focusing, and we need a forth one to compensate for the drift caused by the Z focusing crystal. We have designed the detailed optical model of these configurations to find the combination of active and passive optical elements in the scanning light-path of the microscope, which provides the maximal exploitation of the apertures of all lenses at different X, Y and Z scanning positions, and therefore results in the smallest PSF in the largest possible scanning volume.

Radom-access 3D acousto-optical scanning

To demonstrate 3D imaging at *in vivo* circumstances, I've recorded Ca^{2+} responses from a population of individual neurons in the visual cortex of adult anesthetized mice.

Activity of each neurons were recorded by scanning at 80 Hz, the recorded raw activity was plotted after point-by-point background-correction and normalization, each row showing the activity of a single cell. Responses of neurons could be resolved with high

signal-to-noise ratio. The stability of long-term recording was monitored using the baseline fluorescence.

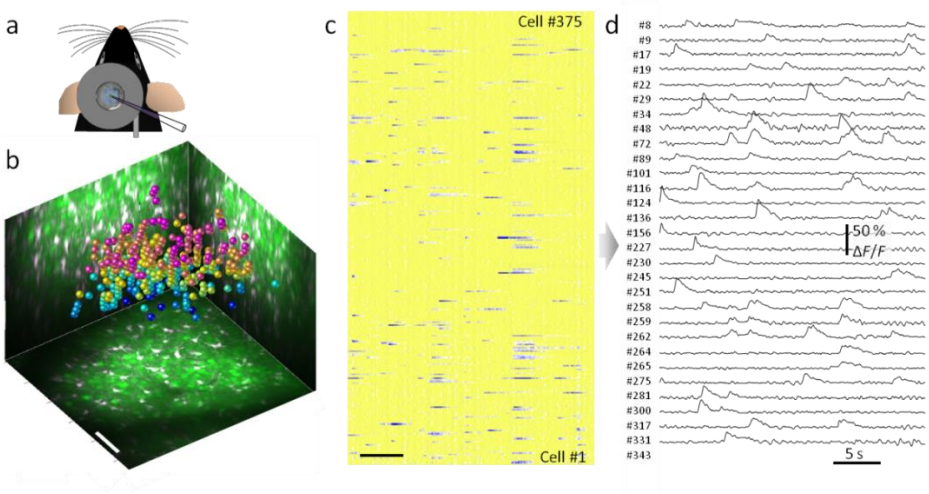

Spontaneous neuronal network activity in vivo. ***(a)*** *Sketch of in vivo experimental arrangement.* ***(b)*** *Maximal intensity side- and z-projection image of the entire z-stack (280×280×230 µm^3; bolus loading with OGB-1-AM and SR-101). Spheres represent 375 autodetected neuronal locations color coded by depth. Scale bars, 50 µm.* ***(c)*** *Parallel 3D recording of spontaneous Ca^{2+} responses from the 375 locations. Rows, single cells measured in random-access scanning mode. Scale bar, 5 s.* ***(d)*** *Examples of Ca^{2+} transients showing active neurons in* ***c****.*

Methods

This documents contains only the summery of the most important methods and discussed in more details in the main text of the thesis.

Mice

The *in vivo* recordings from the primary visual cortex were performed on C57BI/6J, Thy1-Cre, vip/IRES-Cre mice (P60-120). Animals were allowed free access to food and water and were maintained in temperature-, humidity-, and light-controlled conditions. Transgenic lines were developed and bred at the Medical Gene-technological Unit (OGR) of the Institute of Experimental Medicine of the Hungarian Academy of Sciences.

Intrinsic imaging

During *in vivo* imaging and viral injection, the V1 region was localized with intrinsic imaging. For recording intrinsic signal first the skin was opened and the skull over the right hemisphere of the cortex was cleared. The intrinsic signal was recorded using the same visual stimulation protocol we used later during the two-photon imaging session. We could distinguish the region of interest by the absorption change in the given region, as described earlier[1].

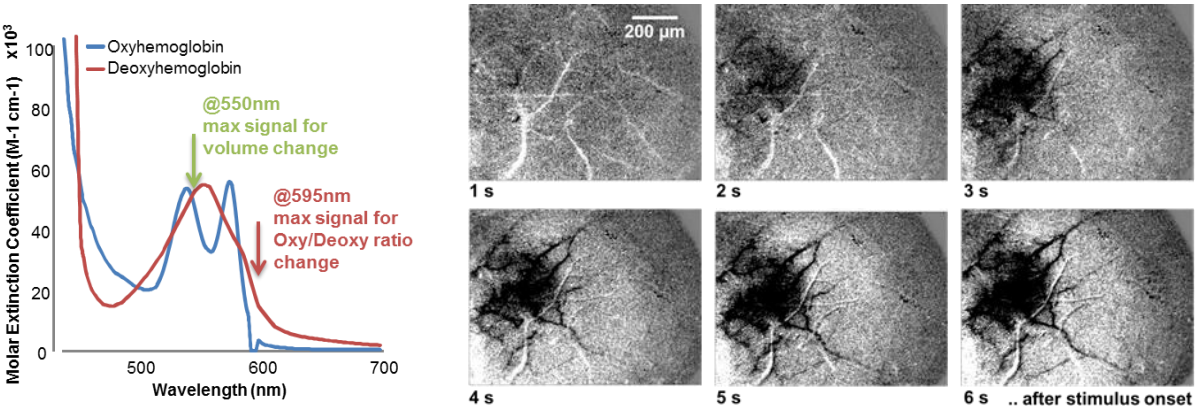

Intrinsic imaging. *Left, absorption spectra of the oxy- and deoxy-hemoglobin shows that the highest relative difference in the absolute absorption of the two states of hemoglobin is present around 595nm, even if the highest absolute signal could have been detected with 550nm illumination. Right, normalized absorption of the brain surface 1-6s after the visual stimulation onset.*

AAV vector injection

The injection procedure was adopted from Chen et al. 2011 and Wertz et al 2015 with some modifications. A 0.5 mm hole was opened in the skull with the tip of a dental drill over the V1 cortical region (centered on average 0.5 mm anterior and 2 mm lateral to the lambda structure – previously localized by intrinsic imaging). The glass micro-pipette (tip diameter ≈10 µm) used for the injections was back-filled with 0.5 µl vector solution (≈6×10^{13} particles/ml) then injected slowly (20 nl/s for first 50 nl, and 2 nl/s for the remaining quantity) into the cortex, at a depth of 450 µm under the pia. For population imaging we used AAV9.Syn.GCaMP6f.WPRE.SV40 or AAV9.Syn.Flex.GCaMP6f.WPRE.SV40 (in the case of Thy-1-Cre animals); both viruses were purchased from Penn Vector Core, Philadelphia, PA. For sparse labeling we injected the 1:1 mixture of AAV9.Syn.Flex.GCaMP6f.WPRE.SV40 and

AAV1.hSyn.Cre.WPRE.hGH diluted 10,000 times. The cranial window was implanted over the injection site 2 weeks after the injection, as described in the surgical procedure section.

Surgical procedure

2-3 weeks after injection, mice were anaesthetized with a mixture of midazolam, fentanyl, and medetomidine (5 mg, 0.05 mg and 0.5 mg/kg body weight, respectively). A circular craniotomy (3 mm diameter) was made above the V1 cortex (localized before virus injection with intrinsic imaging) without touching the dura mater.

A custom-made aluminum head plate was fixed to the skull using cyanoarcylate glue and dental cement.. The area of the craniotomy was covered with a double cover glass, as described previously[2]. Before the imaging sessions, mice were kept head-restrained in the dark under the 3D microscope for at least 1 hour to accommodate to the setup. In some of the animals, a second or third imaging session was carried out after 24 or 48 hours.

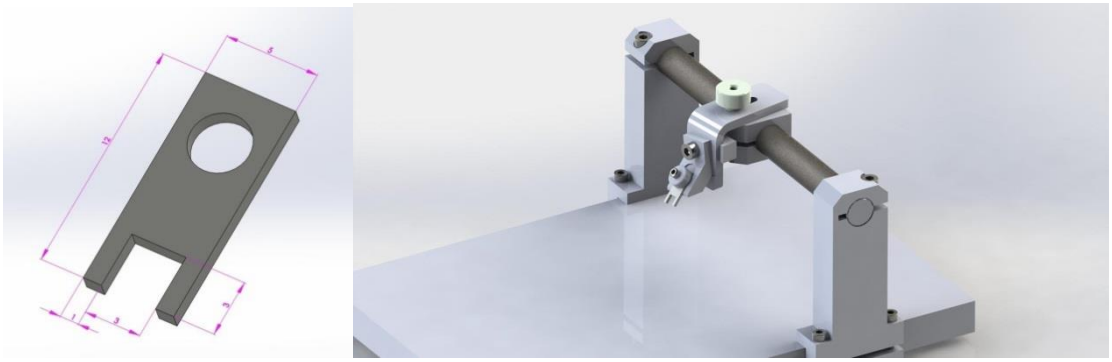

Custom made mouse head holder used during the experiments. *(Left) Headplate mounted to the mouse's skull. (Right) In vivo holder.*

Visual stimulation

A 15" computer monitor (Acer, 1280 x 768 pix resolution) placed 20 centimeters from the contralateral eye (covering ~100° × 70° of the visual field) was used to cast the visual stimuli. To prevent stray light from entering the objective, a black cover was placed over the complete visual stimulation path. Each trial of the visual stimulation started by showing a black screen with a non-moving grating appearing at the edge of the screen after 2 s; after 1 s, the grating moved in a direction orthogonal to its

orientation for 5 s (drifting speed 1 cycle per 1 s), was stopped for 1s, and then disappeared, leaving a black screen for a further 1 s and between the trials. Trials with eight different grating directions were tested with an angular interval of 45°.

In vivo electrophysiology

To determine the correlation between Ca^{2+} transient and AP number, we performed cell-attached patch-clamp recording in *in vivo* conditions. The surgery was as described above, except for a small area left uncovered, about 1 mm wide, next to the cover glasses: this region was used as insertion site for the pipette, while the cells were measured under the cover glass, to limit tissue motion. For the recordings we used 7-8 MΩ-resistance borosilicate glass electrodes filled with extracellular solution, containing (in mM): 126 NaCl, 2.5 KCl, 2 $CaCl_2$, 2 $MgCl_2$, 1.25 NaH_2PO_2, and 100 µM Alexa 594 (Invitrogen) to visualize the pipette. Electrophysiological data were recorded in current-clamp mode with 0 mV holding potential simultaneously with the calcium imaging. Transients were band-pass filtered between 1 Hz and 5 kHz and the number of APs was counted manually.

Data processing

Most of the analysis, including video rearrangement, motion correction, running average and $\Delta F/F$ calculation was performed with the built-in analysis tools in the acquisition software (MES, Femtonics Ltd., Budapest, Hungary). Raw fluorescence data (F) recorded along surface elements in 3D were spatially normalized, and then projected onto a 2D plot by applying the formula: $\Delta F/F = (F(d_L,d_{tr1},t) - F_0(d_L,d_{tr1}))/F_0(d_L,d_{tr1})$, where t denotes time, and d_L and d_{tr1} indicate the longitudinal and the transversal distance along the ribbon, respectively. For 3D projection, 3D rendering, and 3D hyperstack analysis we used the ImageJ open-source software with some custom-written macros.

Aims and results

Despite the evident benefits of 3D random-access AO microscopy, the method faces some limitations when we would like to perform long term measurements from awake, behaving animals, where long term stability and redundancy for motion artefact have key importance. During my work I outlined and addressed these emerging problems and designed novel techniques and measurement strategies which provide stable and reliable image quality for behavioral studies during the everyday use.

Dispersion compensation

Acousto-optical crystals are composed of high refractive index material thus introduce large material dispersion. Therefore, short light pulses (around 100 fs) traveling in high refractive index material are elongated significantly, that reduces two-photon efficiency. In our system with 72 000 fs^2 group delay dispersion (GDD) this effect would produce picosecond long pulses completely diminishing our two-photon signal during *in vivo* measurements. To compensate for this artifact, first we created the detailed optical model of the system containing all the optical elements and calculated the exact material dispersion produced by these components. Then we designed and built a four-prism compressor that fully aborts this error.

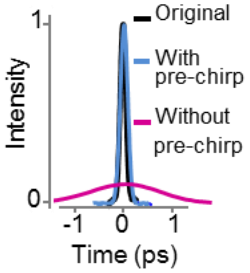

Temporal length of the individual laser pulses at the output of the laser, without and with pulse compression. (Pulse lengths: original – 97fs; with pre-chirp compensation – 108fs; without pre-chirp – 1.4ps)

Besides material dispersion AO crystals also introduce large angular dispersion caused by the spherical inhomogeneity of the AO crystals and other optical elements, which would produce position dependent elongation of the point spread function (PSF). At the edges of the imaging field the extent of this effect can be so large that, on one hand, resolution degrades so even somatas cannot be resolved; on the other hand, laser intensity distributed in a larger focal volume would dramatically reduce quantum efficiency. To compensate for this, the exact properties of the angular dispersion were

determined again from the optical model, and then fully compensated with a special lens introduced in the optical pathway.

Increasing transmittance at longer wavelengths

With the introduction of new genetic dies and sensors in neuroscience (for example GFP or genetically encoded calcium indicators, such as GCaMP6) the use of longer wavelengths became essential to effectively excite these molecules. Acousto-optical cells are highly sensitive to the wavelength and this proportion is inverse. Since we are using four of these crystals in the optical pathway, the transmitted intensity drops dramatically when increasing wavelength. Changing the wavelength from 800 nm to 875 nm, without any additional compensation, would cause the transmittance to drop from 10% to around 1.5%, that is, even with the modern 2-3W femtosecond laser allowing only around 30-45mW imaging power, which is insufficient for *in vivo* measurement deep in the tissue. To overcome this limitation, we applied several optical and electronical developments in the microscope design, to achieve at least as high transmittance as previously with the shorter wavelength.

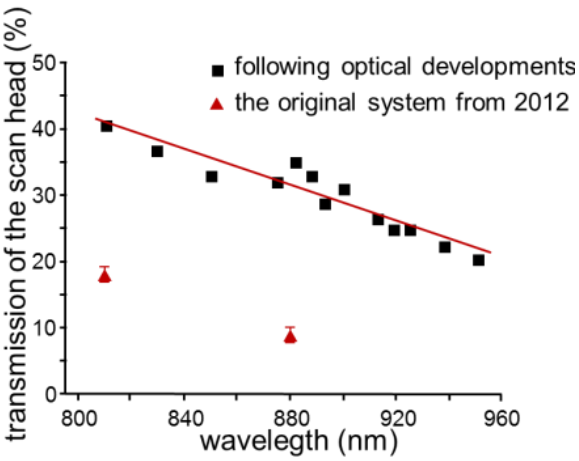

Maximal transmission of the scan head as a function of wavelength (black). The maximal transmission was measured in the center (at x,y,z=0) and decreased as a function of wavelength. Red triangles show transmission of the scan head of the earlier version of the microscope.

AO Drift scanning

Sampling rate is limited by the optical aperture of AO deflectors, which must be filled by an acoustic wave to address a given scanning point. In our system, with relatively large crystal length during 3D point-by-point scanning the switching time is relatively long (about 20-33 µs), which limits either the measurement speed or the number of ROIs. If we are measuring from a behaving animals, therefore have to measure multiple

points per cell or dendritic segment, to produce data for motion correction, with random access point scanning mode the sampling rate would drop to the 1-2 Hz range, which is insufficient to resolve fast Ca^{2+} events.

To resolve this problem we introduce a new scanning method, 3D DRIFT scanning, which increase the scanning rate 3-70 fold depending on the measurement paradigm.

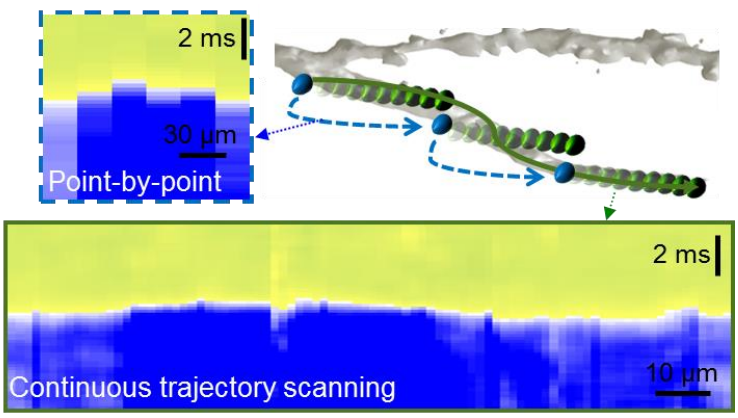

3D DRIFT scanning of dendritic Ca^{2+} spike propagation. *Point-by-point and continuous 3D trajectory scanning of dendritic segments. Top right, schema of the scanning modes (blue point-by-point scanning; green, continuous scanning). Example of Ca^{2+} responses measured by point-by-point (top left) and continuous trajectory modes (bottom). Traces were spatially normalized.*

Motion artefact compensation

It has been shown that neuronal signaling could be completely different in awake and behaving animals. Nevertheless fluorescence data are lost or contaminated with large amplitude movement artifacts during *in vivo* recordings in behaving animals. This occurs because the actual location of the recorded ROIs is continuously changing during the measurements due to tissue movement caused by heartbeats, blood flow in nearby vessels, respiration, and physical motion. This results in fluorescence artifacts because of the spatial inhomogeneity in the baseline fluorescence signal and in relative fluorescence changes. In addition, the amplitudes of motion-induced transients can even be larger than the ones induced by one or a few action potentials detected by genetically encoded calcium indicators (GECIs). Therefore it is difficult to separate post-hoc the genuine fluorescence changes associated with neural activity from the artifacts caused by brain movement. To overcome this problem we used 3D DRIFT AO scanning, extending the pre-selected individual scanning points to small 3D lines, surfaces, or volume elements to cover not only the pre-selected ROIs but also the neighboring background areas or volume elements while maintaining the data sampling rate.

Volume or area images acquired with the methods developed allow motion artifact correction on a fine spatial scale and, hence, the *in vivo* measurement of fine structures in behaving animals. In this way, we can preserve fluorescence information from the pre-selected ROIs during 3D measurements even in the brain of behaving animals, while maintaining the 20-400 Hz sampling rate that is necessary to resolve neural activity at the individual ROIs.

Another source of artifact caused by mechanical instability is the waggle of the beam itself caused by the instability of the optical elements. Reliable microscope stability in the daily routine is a very important factor. Since the optical path of the acousto-optical microscope is more than 6 meters long and containing more than a hundred optical elements, most of them sensitive of temperature and humidity fluctuation, active stabilization of the beam was necessary. This was realized with the combination of quadrant detectors and motorized mirrors.

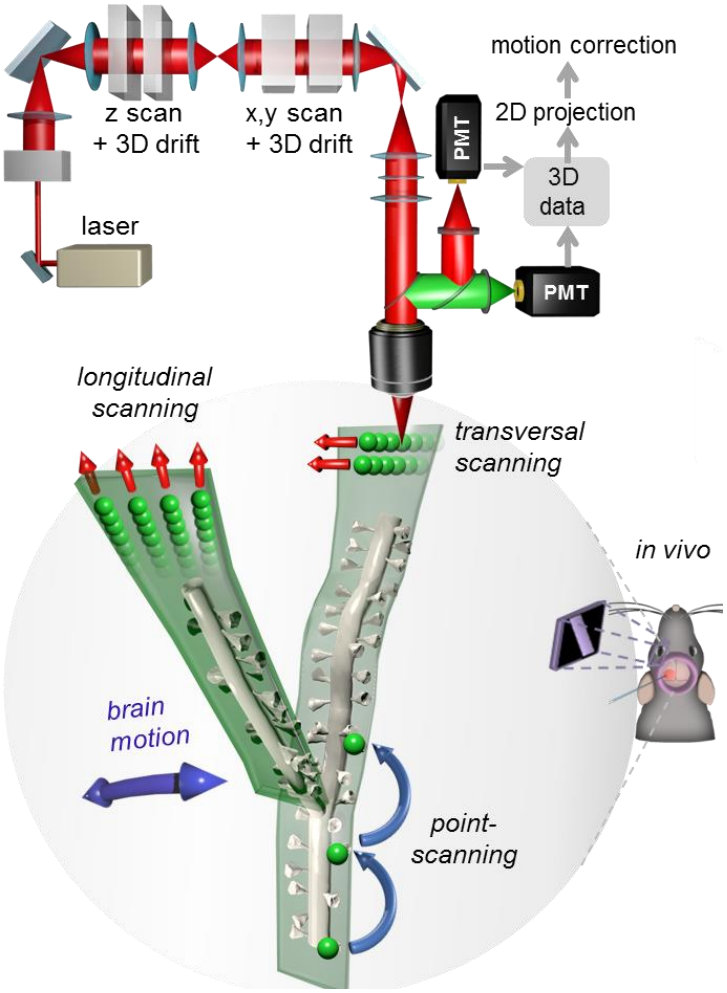

Schematic of the in vivo measurements performed with 3D DRIFT AO microscopy. *In contrast to traditional point-by-point scanning, here the z scanning and x, y scanning units of the microscope can drift the focal spot in 3D in an arbitrary direction and with an arbitrary speed. Therefore, we can extend individual scanning points to a small surface or even volume elements by using, for example, longitudinal or transverse scanning. These surface and volume elements can be set parallel to the average direction of brain movement to preserve fluorescence information for motion correction, even in behaving animals.*

Increased temporal resolution

If we are interested in even faster Ca^{2+} events, such as fine properties of sharpe-wave ripples, local regenerative events or signal propagation along a dendritic arbor, the 20-400 Hz sampling rate of 3D AO point scanning can be still insufficient. This limitation can be overcome at some circumstances, for example, when we have the event repeated many times with very precise timing. Given these circumstances, using random equivalent-time sampling method, we were able resolve sub millisecond or even microsecond events and measure the propagation speed even along a 10-20 μm segment of a dendritic branch.

Discussion

With the optical developments detailed in this work we have improved the optical resolution and transmittance efficiency of the system, also made it possible to image at longer wavelengths, required for imaging of genetically encoded indicators from a field or volume of view up to 500 μm × 500 μm × 650 μm from behaving animals.

With random equivalent-time sampling method using 100 repeats from a given event, we can measure the propagation of a calcium transient along 10-20 μm along a single dendritic segment, allowing the study of signal integration on the subcellular domains. Using this technology, we were able to show the difference of Ca^{2+} signal propagation between room temperature and physiological conditions. The traceable different indicating that the selection of the proper bath temperature might have an influence of the integration properties measured on a dendritic segment.

With the presented novel 3D DRIFT AO scanning technology, we have generated novel 3D scanning methods: 3D ribbon scanning; chessboard scanning; multi-layer, multi-frame imaging; snake scanning; multi-cube scanning; and multi-3D line scanning in large scanning volumes. Our methods allow, for the first time, high-resolution 3D measurements of neuronal networks at the level of tiny neuronal processes, such as spiny dendritic segments, in awake, behaving animals, even under conditions when large-amplitude motion artifacts are generated by physical movement.

Benefits of the new 3D methods in neuroscience

We demonstrate several further technical advances over previous 3D methods in the present work, i) it enables a scanning volume with GECIs which is more than two orders of magnitude larger than previous realizations, while the spatial resolution remains preserved; ii) it offers a method of fast 3D scanning in any direction, with an arbitrary velocity, without any sampling rate limitation; iii) it is free of mechanical and electrical inertias which makes it possible to flexibly select surface and volume elements matching multiple somatic and dendritic locations, thereby effectively focusing measurement time to the ROIs; iv) it compensates fast motion artifacts in 3D to preserve high spatial resolution, characteristic to two-photon microscopy, during 3D surface scanning and volume imaging even in behaving animals; and v) it enables generalization of the low-power temporal oversampling (LOTOS) strategy of 2D raster scanning (Chen et al., 2011) in fast 3D AO measurements to reduce phototoxicity.

When raster scanning of the entire cubature is replaced with 3D DRIFT AO scanning, the $v_{gain} * (SNR_{gain})^2$ is proportional to the ratio of the overall cubature versus the volume covered by the scanned ROIs, and this ratio can be very high (up to 10^6). Therefore, the flexibility in selection of ROIs results in an increase in speed and/or SNR of several orders of magnitude. For example, the measurement of 136 neurons with 25 x 25 frames, instead of imaging the entire cubature, results in an SNR_{gain} that is about 25-fold higher when the measurement speed is constant and, vice versa, the measurement speed is about 600-fold higher while keeping the SNR constant.

These technical achievements enabled the realization of the following fast 3D measurements and analysis methods in awake, behaving animals: i) simultaneous functional recording of over 150 spines; ii) fast parallel imaging of activity in over 12 spiny dendritic segments; iii) precise separation of fast signals in space and time from each individual spine (and dendritic segment) from the recorded volume, in which signals overlap with the currently available methods; iv) simultaneous imaging of large parts of the dendritic arbor and neuronal networks in a z scanning range of over 650 µm; v) imaging a large network of over 100 neurons at subcellular resolution in a scanning volume of up to 500 µm × 500 µm × 650 µm with the SNR more than an order of magnitude larger than for 3D random-access point scanning; and vi) more than 10-fold better single AP resolution during motion in neuronal network measurements.

The limits of our understanding of neural processes lie now at the fast dendritic and neuronal activity patterns occurring in living tissue in 3D, and their integration over larger network volumes. Until now, these aspects of neural circuit function have not been measured in awake, behaving animals. Our new 3D scanning methods, with preserved high spatial and temporal resolution, provide the missing tool for these activity measurements. Among other advantages, it will be possible to use these methods to investigate spike-timing-dependent plasticity and the underlying mechanisms during *in vivo* conditions, the origin of dendritic regenerative activities, the propagation of dendritic spikes, receptive field structures, dendritic computation between multiple spiny and aspiny dendritic segments, spatiotemporal clustering of different input assemblies, associative learning, multisensory integration, the spatial and temporal structure of the activity of spine, dendritic, and somatic assemblies, and function and interaction of sparsely distributed neuronal populations, such as parvalbumin-, somatostatin-, and vasoactive intestinal polypeptide-expressing neurons. These 3D scanning methods may also provide the key to understanding synchronization processes mediated by neuronal circuitry locally and on a larger scale: these are thought to be important in the integrative functions of the nervous system or in different diseases. Importantly, these complex functional questions can be addressed using our methods at the cellular and sub-cellular level, and simultaneously at multiple spiny (or aspiny) dendritic segments, and at the neuronal network level in behaving animals.

Imaging brain activity during motion

Two-dimensional *in vivo* recording of spine Ca^{2+} responses have already been realized in anaesthetized animals and even in running animals, but in these papers only a few spines were recorded with a relatively low SNR. However, fast 2D and 3D imaging of large spine assemblies and spiny dendritic segments in awake, running, and behaving animals has remained a challenge. Yet this need is made clear by recent work showing that the neuronal firing rate more than doubles in most neurons during locomotion, suggesting a completely altered neuronal function in behaving animals. Moreover, the majority of neuronal computation occurs in distant apical and basal dendritic segments which form complex 3D arbors in the brain. However, none of the previous 2D and 3D imaging methods have been able to provide access to these complex and thin (spiny)

dendritic segments during running periods, or in different behavioral experiments, despite the fact that complex behavioral experiments are rapidly spreading in the field of neuroscience. One reason is that, in a typical behavioral experiment, motion-induced fluorescence transients have similar amplitude and kinetics as behavior-related Ca^{2+} transients. Moreover, these transients typically appear at the same time during the tasks, making their separation difficult. Therefore, the 3D scanning methods demonstrated here, alone or in different combinations, will add new tools that have long been missing from the toolkit of neurophotonics for recording dendritic activity in behaving animals.

Compensation of movement of the brain

Although closed-loop motion artifact compensation, with three degrees of freedom, has already been developed at low speed (≈10 Hz), the efficiency of the method has not been demonstrated in awake animals, or in dendritic spine measurements, or at higher speeds characteristic of motion artifacts. Moreover, due to the complex arachnoidal suspension of the brain, and due to the fact that blood vessels generate spatially inhomogeneous pulsation in their local environment, the brain also exhibits significant deformation, not merely translational movements and, therefore, the amplitude of displacement could be different in each and every sub-region imaged. This is crucial when small-amplitude somatic responses (for example single or a few AP-associated responses) or small structures such as dendritic spines are measured. Fortunately, our 3D imaging and the corresponding analysis methods also allow compensation with variable amplitude and direction in each sub-region imaged, meaning that inhomogeneous displacement distributions can therefore be measured and effectively compensated in 3D.

The efficiency of our 3D scanning and motion artifact compensation methods is also validated by the fact that the standard deviation of individual somatic Ca^{2+} transients was largely reduced (up to 20-fold), and became smaller than the amplitude of a single AP-induced transient, especially when multi-cube or chessboard scanning was used. This allows single AP resolution in the moving brain of behaving animals using the currently favored GECI, GCaMP6f. The importance of providing single AP resolution

for neuronal network imaging has also been validated by recent works which have demonstrated that in many systems neuronal populations code information with single APs instead of bursts.

Simultaneous 3D imaging of apical and basal dendritic arbor

Recent data have demonstrated that the apical dendritic tuft of cortical pyramidal neurons is the main target of feedback inputs, where they are amplified by local NMDA spikes to reach the distal dendritic Ca^{2+} and, finally, the somatic sodium integration points where they meet basal inputs also amplified by local NMDA spikes. Therefore, the majority of top-down and bottom-up input integration occurs simultaneously at local integrative computational subunits separated by distances of several hundred micrometers, which demands the simultaneous 3D imaging of neuronal processes in a z range of several hundred micrometers. The maximal, over 1000 μm z-scanning range of AO microscopy, which is limited during *in vivo* measurements with GECIs to about 650 μm by the maximal available power of the currently available lasers, already permitted the simultaneous measurement of apical and basal dendritic segments of layer II/III neurons and dendritic segments of layer V neurons in a range of over 500 μm.

Although 2D imaging in anesthetized animals can capture long neuronal processes[Hiba! A könyvjelző nem létezik.], the location of horizontally oriented long segments is almost exclusively restricted to a few layers (for example to layer I), and in all other regions we typically see only the cross-section or short segments of obliquely or orthogonally oriented dendrites. Moreover, even in cases when we luckily capture multiple short segments with a single focal plane, it is impossible to move the imaged regions along dendrites and branch points to understand the complexity of spatiotemporal integration. The main advantage of the multi-3D ribbon and snake scanning methods is that any ROI can be flexibly selected, shifted, tilted, and aligned to the ROIs; this means that complex dendritic integration processes can be recorded in a spatially and temporally precise manner.

Deep scanning

Although there are many effective methods for fast volume scanning such as SPIM, DSLM-SI, SimView, SCAPE, and OPLUL[Hiba! A könyvjelző nem létezik.], which have broad

application spectra, the z-scanning range of *in vivo* functional measurements in mice is currently limited to about 130 μm in case of these technologies. Imaging deep layer neurons is possible only by either causing mechanical injury or using single-point two-photon or three-photon excitation which allows fluorescent photons scattered from the depth to be collected. One of the main advantages of 3D DRIFT AO scanning is that it is based on whole-field detection, and the extended fast z-scanning range is over 1100 μm in transparent samples and about 650 μm during functional *in vivo* imaging in mouse brain (limited by the power of the laser). Using adaptive optics and regenerative amplifiers can improve resolution and SNR at depth. Moreover, using GaAsP photomultipliers installed directly in the objective arms (travelling detector system) can itself extend the *in vivo* scanning range to over 800 μm. One of the main perspectives of the 3D scanning methods demonstrated here is that the main limitation to reach the maximal scanning ranges of over 1.6 mm[Hiba! A könyvjelző nem létezik.,Hiba! A könyvjelző nem létezik.,Hiba! A könyvjelző nem létezik.] is the relatively low laser intensity of the currently available lasers. Supporting this over a 3 mm z-scanning range has already been demonstrated with 3D AO imaging in transparent samples, where intensity and tissue scattering is not limiting[Hiba! A könyvjelző nem létezik.]. Therefore with future high-power lasers, combined with fast adaptive optics and new red-shifted sensors, may allow a much larger 3D scanning range to be utilized which will, for example, permit the measurement of the entire arbor of deep-layer neurons or 3D hippocampal imaging, without removing any tissue from the cortex.

Although there are several different arrangements of passive optical elements and the four AO deflectors with which it is possible to build microscopes for fast 3D scanning, all of these microscopes use drift compensation with counter-propagating AO waves at the second group of deflectors. The scanning methods demonstrated here can therefore easily be implemented in all 3D AO microscopes. Moreover, at the expense of a reduced scanning volume, 3D AO microscopes could be simplified[Hiba! A könyvjelző nem létezik.] and used as an upgrade in any two-photon system. Hence we anticipate that our new methods will open new horizons in high-resolution *in vivo* imaging in behaving animals.

Credit assignment

I have adopted the methods used in our lab with the help of Daniel Hillier, Attila Kaszás, Linda Judák, Zoltán Szadai and Zoltán Farkas. Pál Maák worked out the design of the acousto optical deflectors, me, Pál Maák, Máté Veress and András Fehér are contributed to the optical design and assemble. I made all calculation and optical design for material dispersion compensation. Calculation for angular dispersion compensation are performed by Pál Maák, realization was performed by all who contributed in the optical assemble. Software and motion correction is written by Gergely Katona and Katalin Ócsai. I have performed all type of measurement listed through the work with the help of Linda Judák, Attila Kaszás and Balázs Chiovini and Balázs Rózsa. Balázs Rózsa, Maák Pál, Gergely Katona and Linda Judák helped me with analysis. Novel scanning method for in vivo motion corrections are designed by me, Gergely Katona and Balázs Rózsa. I have designed and performed both quality increment and motion-detection simulations. In vivo patch clamp measurements were performed by me, Linda Judák and Gábor Juhász.

Publications by the author

1: Szabó Zs, Héja L, Szalay G, Kékesi O, Füredi A, Szebényi K, Dobolyi Á, Orbán TI, Kolacsek O, Tompa T, Miskolczy Zs, Biczók L, Rózsa B, Sarkadi B, Kardos J. Extensive astrocyte synchronization advances neuronal coupling in slow wave activity *in vivo*. Scientific Reports 2017 07 20;7:6018. doi:10.1038/s41598-017-06073-7. **IF: 4.259**

2**: Szalay G*, Judák L*, Katona G*, Ócsai K, Juhász G, Veress M, Szadai Z, Fehér A, Tompa T, Chiovini B, Maák P, Rózsa B. Fast 3D Imaging of Spine, Dendritic, and Neuronal Assemblies in Behaving Animals. Neuron. 2016 Nov 23;92(4):723-738. doi: 10.1016/j.neuron.2016.10.002. PubMed PMID: 27773582. **IF: 13.974**

3: Deneux T, Kaszas A, Szalay G, Katona G, Lakner T, Grinvald A, Rózsa B, Vanzetta I. Accurate spike estimation from noisy calcium signals for ultrafast three-dimensional imaging of large neuronal populations in vivo. Nat Commun. 2016 Jul 19;7:12190. doi: 10.1038/ncomms12190. PubMed PMID: 27432255. **IF: 11.329**

4: Szalay G*, Martinecz B*, Lénárt N, Környei Z, Orsolits B, Judák L, Császár E, Fekete R, West BL, Katona G, Rózsa B, Dénes Á. Microglia protect against brain injury and their selective elimination dysregulates neuronal network activity after stroke. Nat Commun. 2016 May 3;7:11499. doi: 10.1038/ncomms11499. PubMed PMID: 27139776; PubMed Central PMCID: PMC4857403. **IF: 11.329**

5**: Szalay G, Judák L, Szadai Z, Chiovini B, Mezey D, Pálfi D, Madarász M, Ócsai K, Csikor F, Veress M, Maák P, Katona G. [Fast three-dimensional two-photon scanning methods for studying neuronal physiology on cellular and network level]. Orv Hetil. 2016 May 1;157(18):724. doi: 10.1556/650.2016.30457. Hungarian. PubMed PMID: 27106729. **IF: 0.291**

6: Kerekes BP, Tóth K, Kaszás A, Chiovini B, Szadai Z, Szalay G, Pálfi D, Bagó A, Spitzer K, Rózsa B, Ulbert I, Wittner L. Combined two-photon imaging, electrophysiological, and anatomical investigation of the human neocortex in vitro. Neurophotonics. 2014 Jul;1(1):011013. doi: 10.1117/1.NPh.1.1.011013. Epub 2014 Sep 11. PubMed PMID: 26157969; PubMed Central PMCID: PMC4478968. **IF: 5.104**

7: Wertz A, Trenholm S, Yonehara K, Hillier D, Raics Z, Leinweber M, Szalay G, Ghanem A, Keller G, Rózsa B, Conzelmann KK, Roska B. PRESYNAPTIC NETWORKS. Single-cell-initiated monosynaptic tracing reveals layer-specific cortical network modules. Science. 2015 Jul 3;349(6243):70-4. doi: 10.1126/science.aab1687. PubMed PMID: 26138975. **IF: 33.61**

8: Chiovini B, Turi GF, Katona G, Kaszás A, Pálfi D, Maák P, Szalay G, Szabó MF, Szabó G, Szadai Z, Káli S, Rózsa B. Dendritic spikes induce ripples in parvalbumin interneurons during hippocampal sharp waves. Neuron. 2014 May 21;82(4):908-24. doi: 10.1016/j.neuron.2014.04.004. Erratum in: Neuron. 2014 Aug 6;83(3):749. PubMed PMID: 24853946. **IF: 13.974**

9**: Katona G*, Szalay G*, Maák P*, Kaszás A*, Veress M, Hillier D, Chiovini B, Vizi ES, Roska B, Rózsa B. Fast two-photon in vivo imaging with three-dimensional random-access scanning in large tissue volumes. Nat Methods. 2012 Jan 8;9(2):201-8. doi: 10.1038/nmeth.1851. PubMed PMID: 22231641. **IF: 23.565**

* These authors contributed equally to the publications.
** The result from this articles are presented in this thesis.

References

[1] Cang J, Kalatsky VA, Lowel S, Stryker MP (2008) Optical imaging of the intrinsic signal as a measure of cortical plasticity in the mouse. Visual Neuroscience 22:685-691.

[2] Goldey GJ, Roumis DK, Glickfeld LL, Kerlin AM, Reid RC, Bonin V, Schafer DP, Andermann ML (2014) Removable cranial windows for long-term imaging in awake mice. Nature protocols 9:2515-2538.